Magnetostratigraphy, paleomagnetic correlation, and deformation of Pleistocene deposits in the south central Puget Lowland, Washington

Jonathan T. Hagstrum,[1] Derek B. Booth,[2] Kathy G. Troost,[3] and Richard J. Blakely[1]

[1] Paleomagnetic results from Pleistocene sedimentary deposits in the central Puget Lowland indicate that the region has experienced widespread deformation within the last 780 kyr. Three oriented samples were collected from unaltered fine-grained sediments mostly at sea level to determine the magnetostratigraphy at 83 sites. Of these, 47 have normal, 18 have reversed, and 18 have transitional (8 localities) polarities. Records of reversed- to normal-polarity transitions of the geomagnetic field were found in thick sections of silt near the eastern end of the Tacoma Narrows Bridge, and again at Wingehaven Park near the northern tip of Vashon Island. The transitional horizons, probably related to the Bruhnes-Matuyama reversal, apparently fall between previously dated Pleistocene sediments at the Puyallup Valley type section (all reversed-polarity) to the south and the Whidbey Island type section (all normal-polarity) to the north. The samples, in general, are of sufficient quality to record paleosecular variation (PSV) of the geomagnetic field, and a statistical technique is used to correlate horizons with significant agreement in their paleomagnetic directions. Our data are consistent with the broad structures of the Seattle uplift inferred at depth from seismic reflection, gravity, and aeromagnetic profiles, but the magnitude of vertical adjustments is greatly subdued in the Pleistocene deposits.   *INDEX TERMS:* 1520 Geomagnetism and Paleomagnetism: Magnetostratigraphy; 1522 Geomagnetism and Paleomagnetism: Paleomagnetic secular variation; 1525 Geomagnetism and Paleomagnetism: Paleomagnetism applied to tectonics (regional, global); 1535 Geomagnetism and Paleomagnetism: Reversals (process, timescale, magnetostratigraphy); *KEYWORDS:* Puget Lowland, Pleistocene, magnetostratigraphy, paleosecular variation, tectonic deformation

1. Introduction

[2] The heavily populated Puget Lowland region (Figure 1) has been the subject of an increasing number of scientific investigations designed to clarify the nature of its seismic hazards. The lowland has had a large number of historical earthquakes relative to its surrounding areas, and most of the larger events have been within the subducting Juan de Fuca plate [*Ludwin et al.*, 1991; *Rogers et al.*, 1996]. Recent geologic investigations, however, have documented major prehistoric earthquakes in the overriding North American plate, in particular along the Seattle fault [*Bucknam et al.*, 1992; *Nelson et al.*, 1999]. Considering the potential consequences of a large earthquake in the modern Puget Lowland, relatively little information is available concerning the region's basic structural setting and paleoseismicity. Understanding the stratigraphy, structure, and deformation of Quaternary sedimentary deposits within the Puget Lowland is important for an accurate assessment of the region's seismic hazards.

[3] Geologic mapping in the mostly unconsolidated sedimentary cover of the Puget Lowland is difficult primarily because of similar appearances of various Pleistocene glacial and nonglacial deposits mantling the area and poor exposure caused by abundant landslide deposits, dense vegetation, and urban development. We report here on a magnetostratigraphic study that was initially undertaken to provide a rudimentary understanding of the regional Pleistocene stratigraphy: reversed(R)-polarity paleomagnetic directions are assumed to indicate an age greater than ~780 ka and normal(N)-polarity directions an age less than ~780 ka, the Bruhnes-Matuyama boundary.

[4] The paleomagnetic data are apparently of sufficient quality, however, that paleosecular variation (PSV) of the geomagnetic field was recorded. Significant parts of a polarity reversal, probably the Bruhnes-Matuyama transition, are recorded at localities near the eastern end of The Tacoma Narrows Bridge and at Wingehaven Park near the northeastern end of Vashon Island (Figure 1). Transitional directions are found at a number of other sites and potentially provide a high-precision stratigraphic marker horizon. Furthermore, similar PSV directions for sites of N, transitional, and R polarity have been correlated using a statistical technique developed by *Bogue and Coe* [1981]. Finally, we compare our paleomagnetic results with structural models developed using seismic reflection profiles beneath Puget Sound [*Pratt et al.*, 1997] and tomographic data from the 1998 Seismic Hazards Investigation in Puget Sound (SHIPS [*Brocher et al.*, 2001]).

2. Geologic Setting

[5] The oceanic Juan de Fuca plate is the northernmost remnant of the Farallon plate subducting beneath North America, and its oblique convergence with the continental margin is the source of great subduction zone earthquakes [*Atwater and Hemphill-Haley*, 1997], complex upper plate folding and faulting [*Johnson et al.*, 1999], and Cascade arc volcanism [*Smith*, 1993]. On the basis of Neogene deformation, paleomagnetic rotations, and geodetic data the Cascadia forearc appears to be migrating northward and breaking up into large rotating blocks associated with dextral transpression [*Wells et al.*, 1998]. The

---

[1]U.S. Geological Survey, Menlo Park, California, USA.
[2]Department of Earth and Space Sciences, University of Washington, Seattle, Washington, USA.
[3]Department of Geological Sciences, University of Washington, Seattle, Washington, USA.
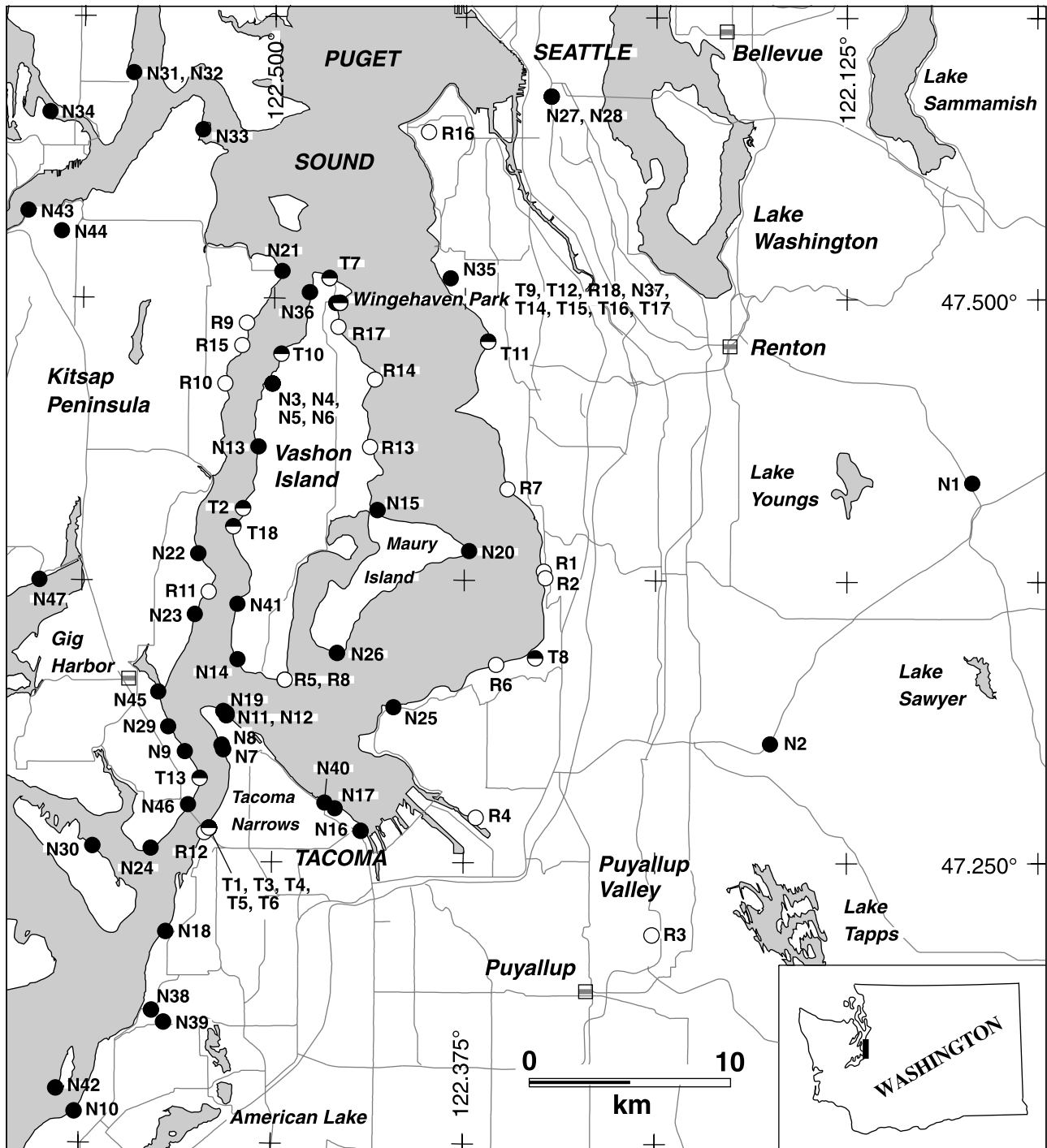
Figure 1. Map of central Puget Lowland showing paleomagnetic sampling sites (circles). Solid circles indicate sites with normal-polarity remanent magnetizations, open circles indicate sites with reversed-polarity magnetizations, and half-solid circles indicate sites with transitional-polarity directions (Table 1). Inset at the lower right shows the location of the central Puget Lowland in Washington State.

Puget Lowland lies within this transpressional zone in northwestern Washington, overlying a major crustal boundary between Eocene basement rocks of the western Coast Range province and pre-Tertiary rocks of the eastern Cascade province [*Wells and Coe*, 1985; *Johnson et al.*, 1996].

[6] Seismic reflection profiles beneath Puget Sound indicate subhorizontal Paleogene and Neogene sedimentary rocks deformed by west to northwest trending faults and folds [*Pratt et al.*, 1997].

The stratigraphy in the lowland consists of the Crescent Formation basalts overlain in the Seattle basin by upper Eocene marine sedimentary strata, shallow-marine turbidites of the upper Eocene to Oligocene Blakeley Formation, by nonmarine Miocene sediments of the Blakely Harbor Formation, and by Quaternary deposits. Asymmetric subsidence of the Seattle basin indicates continued contractional deformation since Eocene time [*Johnson et al.*, 1994].
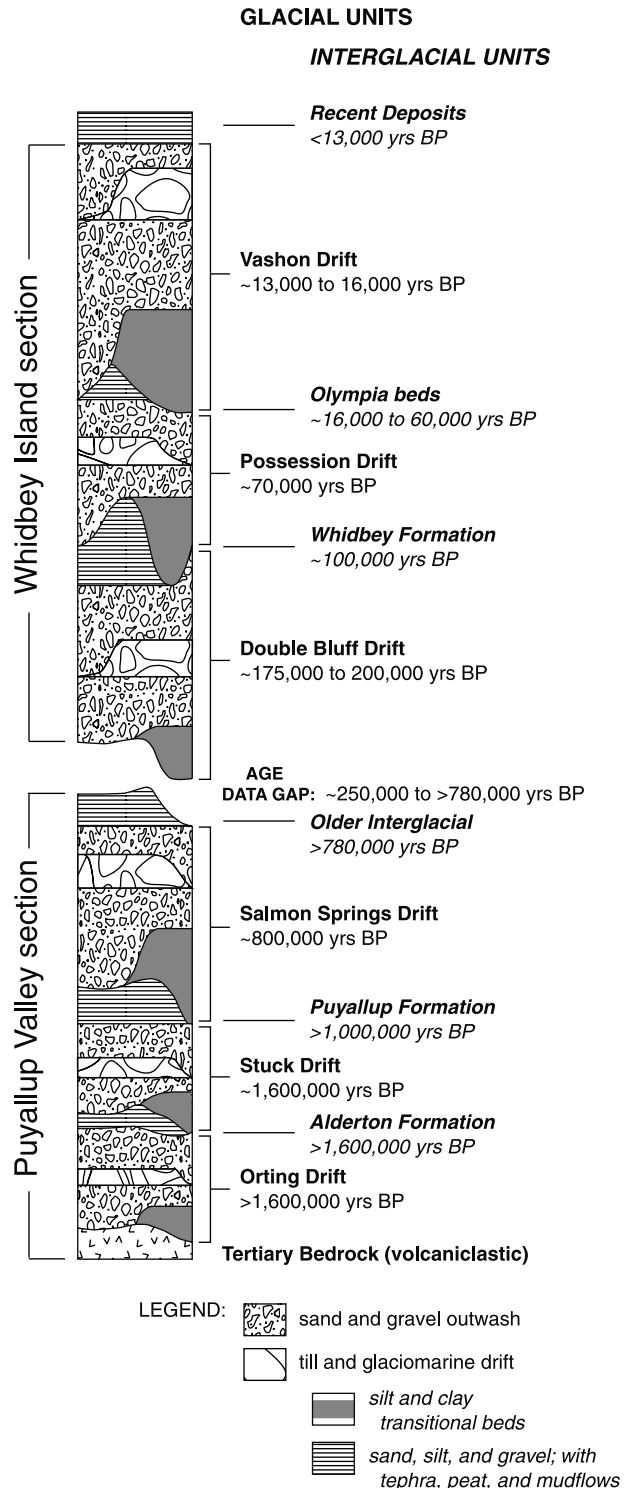
[7] A primary subsurface feature is the Seattle uplift, with south dipping (∼20°) bedrock strata on its south flank, and steeply north dipping (50°−90°) strata and the east trending Seattle fault on its north flank. *Pratt et al.* [1997] interpreted this and other uplifts as fault-bend and fault-propagation folds, and suggested that the Puget Lowland is underlain by a large, north directed thrust sheet (thin-skinned deformation) bounded by faults along the Cascade and Olympic Ranges to the east and west [*Johnson et al.*, 1994], respectively. *Brocher et al.* [2001], on the other hand, interpret the Seattle uplift as a pop-up structure [*Wells and Weaver*, 1993] bounded by the steeply dipping Seattle fault to the north and the Tacoma fault to the south. The Tacoma fault is inferred from gravity and magnetic data and a seismic velocity gradient similar to that associated with the Seattle fault. In addition, the Tacoma fault is inferred from the magnitude of structural relief along this zone, particularly to the west. Conversely, structural relief along the Seattle fault zone decreases to the west, and *Brocher et al.* [2001] suggest that this relationship likely results from the transfer of strain between the Seattle and Tacoma faults.

[8] The glacial and interglacial deposits overlying Tertiary basement rocks in the southern Puget Lowland (Figure 2) indicate that the area was glaciated at least 6 times during the Pleistocene Epoch [*Easterbrook*, 1994]. Near Tacoma, these deposits are ∼400 m thick [*Jones*, 1996]. Correlations between units have been difficult to make due to the lack of distinctive lithologic or textural features and to problems in dating materials of this composition and age. More recently, laser-argon, fission track, thermoluminescence, amino acid, and paleomagnetic techniques have been employed to establish a chronology for these Pleistocene sediments, particularly north and east of the Seattle-Tacoma area [*Blunt et al.*, 1987; *Easterbrook*, 1994; *Troost*, 1999; *Troost and Booth*, 1999].

[9] The last glacial advance in the Puget Lowland was the Puget lobe of the Cordilleran Ice Sheet, culminating ∼15 kyr ago during the Vashon stade of the Fraser glaciation [*Booth*, 1987]. In the Puyallup River valley, one of the type sections of older, pre-Vashon glacial and nonglacial deposits is exposed (Figure 2). It consists of drift and outwash of the Orting, Stuck, and Salmon Springs glaciations [*Crandell et al.*, 1958]. All of these glacial materials and their interbedded nonglacial deposits have R-polarity remanent magnetizations and ages greater than ∼780 ka [*Easterbrook et al.*, 1988; *Easterbrook*, 1994]. To the north on Whidbey Island (∼50 km north of Seattle), the upper type section of Pleistocene deposits (Figure 2) consists of the Double Bluff, Possession, and Vashon glacial deposits and intervening glacial and nonglacial deposits [*Easterbrook et al.*, 1967]. Here the entire section has N-polarity magnetizations and ages less than ∼780 ka [*Easterbrook*, 1994]. No deposits between the Double Bluff and Salmon Springs glaciations (Figure 2) have yet been identified in the Puget Lowland [*Richmond and Fullerton*, 1986]. Mapping efforts in the Tacoma area have identified the Vashon glacial drift and at least two older drifts of N polarity (this study) which may fall between the Double Bluff and Salmon Springs deposits based on preliminary luminescence dates [*Troost*, 1999; *Mahan et al.*, 2000].

3. Magnetostratigraphy

[10] Generally, three oriented samples were collected from unweathered (dark gray), fine-grained (silt) glacial and interglacial lake deposits (Figure 2) at each of 86 sites in the central Puget Lowland. Horizontal benches were excavated and leveled with a circular bubble level, and then vertical pedestals were carved over which plastic sample boxes (volume of 6 cm³) were fitted. Before removal, one top edge of each box was marked and oriented using a magnetic compass. Local bedding was also recorded to correct for deformation since original deposition. The sites are mostly at sea

GLACIAL UNITS

INTERGLACIAL UNITS

Recent Deposits
<13,000 yrs BP

Vashon Drift
∼13,000 to 16,000 yrs BP

Olympia beds
∼16,000 to 60,000 yrs BP

Possession Drift
∼70,000 yrs BP

Whidbey Formation
∼100,000 yrs BP

Double Bluff Drift
∼175,000 to 200,000 yrs BP

**AGE
DATA GAP:** ∼250,000 to >780,000 yrs BP

Older Interglacial
>780,000 yrs BP

Salmon Springs Drift
∼800,000 yrs BP

Puyallup Formation
>1,000,000 yrs BP

Stuck Drift
∼1,600,000 yrs BP

Alderton Formation
>1,600,000 yrs BP

Orting Drift
>1,600,000 yrs BP

Tertiary Bedrock (volcaniclastic)

Whidbey Island section

Puyallup Valley section

LEGEND:

    sand and gravel outwash

    till and glaciomarine drift

    *silt and clay
    transitional beds*

    *sand, silt, and gravel; with
    tephra, peat, and mudflows*

Figure 2. Conceptual Quaternary stratigraphic framework for the Puget Lowland showing the younger Whidbey Island type section [*Easterbrook et al.*, 1967] with the addition of the Olympia beds [*Troost*, 1999] and the older Puyallap Valley type section [*Crandell et al.*, 1958]. At present, an age data gap exists between the older reversed-polarity section (>780 ka) and the younger normal-polarity section (< ∼ 250 ka). Modified from *Troost* [1999].

level in beach exposures around Puget Sound, but some were also collected in road-cut (N3−N6, N16, N17, R12, N27, N28, N37, N38, N40), stream bank (N1, N2, R16, N39, N44), and hillside (R3, T1, T3−T6, T8, N35, N46) exposures (Figure 1 and Table 1).

Table 1. Paleomagnetic Data for Fine-Grained Glacial Deposits in the Puget Sound Region, Washington[a]

Site	Lab ID	Location	Elev., m	λ_S, deg	ϕ_S, deg	Strike/Dip	I, deg	D, deg	N/N_0	R	k	α_{95}	λ_P, deg	ϕ_P, deg
						Normal Polarity								
N1	T6089	Cedar River	80	47.419	122.043	0/0	54.5	4.0	3/3	2.9911	224	8.3	88.8	222.2
N2	T6092	Green River	21	47.303	122.175	0/0	79.1	359.2	3/3	[−2359,−45]	[1.2,11.4]		68.3	237.0
N3	T7001	Christiansen Road	20	47.462	122.501	0/0	47.0	351.3	3/3	2.9737	76	14.2	69.6	80.0
N4	T7004	Christiansen Road	26	47.462	122.501	0/0	72.3	23.1	3/3	2.9450	36	20.8	72.9	283.3
N5	T7007	Christiansen Road	30	47.462	122.501	0/0	39.3	338.2	3/3	2.8747	16	31.9	59.3	99.9
N6	T7010	Christiansen Road	50	47.462	122.501	0/0	80.8	33.0	2/2	1.9999	–	–	61.1	257.8
N7	T7018	Salmon Beach	<2	47.300	122.532	0/0	55.2	348.6	3/3	2.9978	902	4.1	75.7	97.8
N8	T7021	Salmon Beach	<2	47.302	122.533	0/0	39.4	329.9	3/3	2.9914	233	8.1	55.3	112.0
N9	T7024	north of Point Evans	<2	47.299	122.557	0/0	28.2	20.1	3/3	2.9964	559	5.2	53.7	23.4
N10	T7027	Solo Point	18	47.139	122.628	0/0	57.6	358.2	3/3	2.9973	752	4.5	81.0	66.4
N11	T7030	Point Defiance	2	47.315	122.530	160/7	36.0	339.8	3/3	2.9990	1897	2.8	66.3	91.0
N12	T7033	Point Defiance	<2	47.316	122.530	130/3	61.5	358.9	3/3	2.9993	2782	2.3	85.4	51.9
N13	T7277	Sunset Beach	<2	47.434	122.510	0/0	69.8	257.9	3/3	2.9029	21	27.9	30.6	195.2
N14	T7283	Spring Beach	<2	47.340	122.523	0/0	51.3	36.2	3/3	2.9644	56	16.6	58.6	343.6
N15	T7289	Portage	<2	47.406	122.432	0/0	31.5	11.3	3/3	2.9744	78	14.0	58.2	36.7
N16	T7292	Schuster Parkway	6	47.264	122.442	0/0	56.2	275.4	3/3	2.9940	336	6.7	29.4	171.3
N17	T7295	Garfield Park	12	47.274	122.459	0/0	68.5	322.8	3/3	2.9876	161	9.7	65.7	172.1
N18	T7307	Sunset Beach	24	47.219	122.569	0/0	50.4	355.4	3/3	2.9694	65	15.4	73.6	71.5
N19	T8101	Point Defiance	0	47.317	122.532	0/0	31.0	308.9	3/3	2.9981	1061	3.8	38.3	129.1
N20	T8107	Point Robinson	<2	47.388	122.372	0/0	61.6	306.9	3/3	2.9993	2931	2.3	53.0	160.6
N21	T8194	Southworth	<2	47.512	122.495	0/0	52.2	305.0	3/3	2.9773	88	13.2	46.5	148.4
N22	T8203	north of Point Richmond	18	47.387	122.549	0/0	71.6	307.5	3/3	2.9988	1606	3.1	57.3	183.1
N23	T8209	Sunrise	5	47.360	122.551	0/0	36.9	298.9	3/3	2.9844	128	10.9	34.4	140.9
N24	T8218	Point Fosdick	<2	47.256	122.579	0/0	36.7	291.6	3/3	2.9909	220	8.3	29.4	146.4
N25	T8221	Dash Point State Park	<2	47.319	122.421	0/0	49.5	40.3	3/3	2.9046	21	27.6	54.8	341.8
N26	T8230	Piner Point	<2	47.343	122.458	0/0	68.3	272.4	3/3	2.9843	127	11.0	36.4	186.9
N27	T9013	I−5 at Atlantic Street	25	47.590	122.319	310/15	27.0	352.4	2/3	1.9633	–	–	49.6	73.2
N28	T9016	I−5 at Atlantic Street	25	47.590	122.319	170/15	38.3	23.2	3/3	2.9994	3342	2.1	50.9	349.8
N29	T9061	Shore Acres	<2	47.310	122.568	165/5	50.2	12.6	3/3	2.9953	427	6.0	69.0	3.3
N30	T9064	Fox Island	<2	47.257	122.617	0/0	60.1	352.8	3/3	2.9738	76	14.2	81.9	99.7
N31	T0049	Illahee State Park	<2	47.599	122.593	0/0	60.6	298.2	3/3	2.9749	80	13.9	46.7	163.2
N32	T0052	Illahee State Park	3	47.599	122.593	0/0	60.0	323.2	3/3	2.9935	306	7.1	63.1	146.6
N33	T0058	Manchester St. Park	<2	47.575	122.546	130/30	58.2	283.8	3/3	2.9951	404	6.1	36.1	168.2
N34	T0061	Anderson Cove	<2	47.583	122.649	0/0	61.2	5.3	3/3	2.9833	120	11.3	83.5	19.9
N35	T0130	47th Street landslide	72	47.509	122.388	60/12	61.3	11.0	3/3	2.9388	33	21.9	80.7	356.9
N36	T0139	Sylvan Beach	<2	47.501	122.477	0/0	49.8	302.8	3/3	2.9819	111	11.8	43.6	147.5
N37	T0145	Wingehaven Park	24	47.497	122.463	0/0	60.7	357.5	3/3	2.9972	724	4.6	83.9	75.7
N38	T0148	Abitibi Paper Co.	30	47.185	122.577	230/4	58.5	290.7	3/3	2.9961	512	5.5	40.5	164.9
N39	T0151	Garrison Creek	46	47.180	122.569	0/0	33.6	342.2	3/3	2.9904	208	8.6	57.7	90.3
N40	T0154	Puget Gardens	8	47.279	122.674	95/12	37.4	2.3	2/3	1.9927	–	–	63.6	52.7
N41	T0157	Camp Sealth	<2	47.362	122.525	0/0	29.6	344.1	3/3	2.9799	100	12.4	55.9	85.5
N42	T0208	Ketron Island	<2	47.149	122.661	0/0	61.6	348.9	3/3	2.9971	681	4.7	81.0	122.1
N43	T0241	Ross Point	8	47.538	122.664	0/0	60.5	0.6	3/3	2.8920	19	29.5	83.9	53.1
N44	PH001	Blackjack Creek	30	47.523	122.638	345/27	55.0	41.3	3/3	2.9879	165	9.6	57.3	333.6
N45	T1300	Gig Harbor	<2	47.324	122.576	125/8	40.7	289.2	3/3	[−33,−2]	[12.1,19.1]		29.7	150.4
N46	T1306	Tacoma Narrows	12	47.276	122.555	235/25	28.7	337.2	3/3	2.9209	25	25.1	52.9	95.7
N47	T1348	Wauna	<2	47.376	122.653	115/15	78.5	354.3	3/3	2.9813	107	12.0	69.3	231.3
		Average		47.370	122.450		57.5	341.4	47/47	42.7229	11	6.6	73.5	120.0
						Transitional Polarity								
T1	T7015	Tacoma Narrows	27	47.265	122.541	0/0	−22.7	21.1	3/3	2.9835	121	11.3	28.0	33.9
T2	T7280	Lisabeula	<2	47.407	122.520	0/30	15.4	13.6	3/3	2.9906	213	8.5	48.8	36.8
T3	T7298	Tacoma Narrows	26	47.265	122.541	0/0	−39.2	316.5	3/3	[−1071,−3]	[1.9,4.6]		10.3	97.9
T4	T7301	Tacoma Narrows	28	47.265	122.541	0/0	−7.7	24.2	3/3	2.9969	647	4.9	34.6	27.7
T5	T7304	Tacoma Narrows	28	47.265	122.541	00	−4.1	15.2	3/3	2.9822	112	11.7	38.9	37.8
T6	T8212	Tacoma Narrows	26	47.265	122.541	0/0	−30.0	342.5	3/3	2.9912	228	8.2	24.7	76.0
T7	T8224	Vashon Ferry Dock	<2	47.509	122.464	0/0	−11.8	347.9	3/3	2.9906	212	8.5	35.5	72.4
T8	T9043	Redondo	40	47.341	122.328	350/12	21.4	354.4	3/3	2.9930	284	7.3	40.7	76.2
T9	T9046	Wingehaven Park	<2	47.498	122.457	0/0	8.6	11.1	3/3	2.9425	35	21.2	45.8	41.6
T10	T9049	Peter Point	<2	47.476	122.495	260/4	17.3	334.5	3/3	2.9966	590	5.1	48.4	92.5
T11	T9055	Seahurst Park	<2	47.481	122.360	0/0	8.5	348.7	3/3	[−42,−1]	[11.0,15.8]		45.7	73.8
T12	T0133	Wingehaven Park	3	47.498	122.457	0/0	12.1	14.6	3/3	2.9862	144	10.3	46.8	36.1
T13	T1303	Tacoma Narrows	<2	47.289	122.549	95/11	8.0	349.2	3/3	2.9948	383	6.3	45.7	73.0
T14	T1309	Wingehaven Park	3	47.498	122.457	0/0	1.9	22.0	3/3	2.9898	195	8.8	39.7	28.4
T15	T1312	Wingehaven Park	3	47.498	122.457	0/0	−3.5	18.5	3/3	2.9725	73	14.6	38.2	33.8
T16	T1315	Wingehaven Park	2	47.498	122.457	0/0	34.7	31.0	3/3	2.9684	63	15.6	52.1	5.3
T17	T1318	Wingehaven Park	<2	47.498	122.457	0/0	3.7	6.2	3/3	2.9906	212	8.5	44.0	48.9
T18	T1321	Sanford Point	<2	47.399	122.526	240/11	8.3	4.7	3/3	2.9477	38	20.2	46.6	50.6

Table 1. (continued)

Site	Lab ID	Location	Elev., m	λ_S, deg	ϕ_S, deg	Strike/Dip	I, deg	D, deg	N/N_0	R	k	α_{95}	λ_P, deg	ϕ_P, deg
						Reversed Polarity								
R1	T6079	Saltwater State Park	<2	47.379	122.323	0/0	−62.7	156.1	5/5	4.8596	28	14.6	73.1	145.3
R2	T6084	Saltwater State Park	<2	47.376	122.322	0/0	−76.2	140.2	5/5	4.9823	226	5.1	63.2	199.0
R3	T6095	Sumner	34	47.218	122.252	0/0	−10.4	157.1	3/3	[−208,−33]	[4.0,38.7]		43.7	90.1
R4	T7012	Jones East	5	47.270	122.367	0/0	−71.2	210.5	3/3	[−14719,−5]	[0.5,1.5]		69.4	291.9
R5	T7286	Neill Point	<2	47.331	122.492	250/20	−25.5	168.4	3/3	2.6233	5	−	63.6	46.3
R6	T7310	Adelaide	<2	47.338	122.354	0/0	−42.0	182.7	3/3	2.9489	39	20.0	66.8	51.4
R7	T8098	Marine View Park	<2	47.416	122.347	0/0	−71.1	150.7	3/3	[−419,−5]	[3.0,8.8]		70.2	183.1
R8	T8104	Neill Point	<2	47.331	122.492	245/12	−25.6	113.9	3/3	[−383,−9]	[3.0,12.8]		38.4	145.7
R9	T8197	Driftwood Cove	<2	47.489	122.518	0/0	−51.2	153.0	3/3	[−6140,−63]	[0.7,8.3]		64.2	119.9
R10	T8200	Fragaria Beach	3	47.462	122.532	0/0	−85.1	228.2	3/3	[−7098,−7]	[0.7,2.6]		53.4	249.8
R11	T8206	Kingfish	<2	47.370	122.542	0/0	−37.7	223.9	3/3	[−1288,−23]	[1.6,11.1]		46.1	348.6
R12	T8215	Tacoma Narrows	5	47.263	122.544	0/0	−37.3	161.6	3/3	[−827,−20]	[2.0,12.9]		59.7	93.2
R13	T8227	Klahanie	<2	47.434	122.437	0/0	−42.1	187.7	3/3	[−27220,−2]	[0.4,0.7]		66.1	40.1
R14	T9052	Point Beals	<2	47.464	122.434	280/20	−45.3	151.9	3/3	[−180,−27]	[4.3,36.5]		59.8	114.4
R15	T9058	View Park South	30	47.479	122.521	0/0	−71.6	203.3	3/3	[−6476,−21]	[0.7,4.7]		73.2	286.9
R16	T0127	Schmitz Park	37	47.576	122.400	30/12	−57.6	207.6	3/3	[−140,−6]	[5.1,17.6]		67.9	342.4
R17	T0136	127th Avenue Beach	<2	47.489	122.460	0/0	−63.2	151.4	3/3	[−28,−19]	[11.3,20.-4]		70.1	150.3
R18	T0142	Wingehaven Park	<2	47.498	122.457	0/0	−44.4	190.8	3/3	[−514,−2]	[2.9,5.2]		67.0	32.2
		Average		47.370	122.450		−55.1	166.3	18/18	16.0836	9	12.3	74.4	103.4
		N+R average		47.370	122.450		56.8	342.8	65/65	58.7831	10	5.8	73.9	115.6

[a] Site, site ID used throughout this report; Lab ID, laboratory identification number of paleomagnetic sampling site; Elev., elevation of site; λ_S and ϕ_S are north latitude and west longitude of site; Strike and dip of bedding, dip is 90° clockwise of strike; I and D are inclination and declination of mean paleomagnetic directions corrected for strike and dip; N/N_0 is number of samples averaged/number of samples collected; R is vector sum of N unit vectors; k is concentration parameter [*Fisher*, 1953]; α_{95} is radius of 95% confidence in degrees; for means calculated using Bingham statistics, R is not calculated, $[−k_1/−k_2]$ are the two Bingham concentration parameters, and $[\alpha_1/\ \alpha_2]$ are the two Bingham 95% confidence limits [*Onstott*, 1980]; λ_P and ϕ_P are north latitude and east longitude of virtual geomagnetic pole. The expected present-day normal and reversed field directions for the Puget Sound area are $I = 69.7°$, $D = 20.2°$ and $I = −69.7°$, $D = 200.2°$, respectively; the expected dipole direction is $I = 65.3°$, $D = 0°$.

[11] Stepwise alternating field demagnetization indicates that these sediments carry stable characteristic remanent magnetizations (Figures 3a and 3b). Three sites with unstable magnetizations were discarded from further analysis. The normal-polarity characteristic magnetization vectors were usually isolated between 20 and 100 mT. Least squares lines are fitted to the sample demagnetization data [*Kirschvink*, 1980], and *Fisher* [1953] statistics are calculated for single-component site-mean directions and for the overall mean directions. For R-polarity samples, N-polarity components were first removed or, more often, the N-polarity overprint was removed simultaneously with the characteristic R-polarity component. Converging demagnetization planes and Bingham statistics [*Onstott*, 1980], therefore, were used to determine the characteristic magnetization direction and error limits, respectively, for most of the R-polarity sites (Figure 3c).

[12] In this procedure, great circles were fitted to the demagnetization endpoint data that are curved rather than linear in vector plots due to overlapping coercivities for the two components of remanent magnetization. The great circles are expected to intersect at the component's direction having the higher coercivity range. The technique works best if the lower-coercivity components have random directions, making the statistical certainty of the characteristic direction greater and its 95% confidence limits correspondingly smaller and more circular. If both components are nonrandom, however, the intersection point of the great circles might be nearer the higher-coercivity direction or the antipode of the lower-coercivity direction, depending on how well the directions are represented by the sample population. In such cases, the error ellipses are more elongate (Figure 4), and the mean directions are less reliable.

[13] Samples from 47 sites have N-polarity mean directions, 18 sites have R-polarity directions, and 18 sites (8 localities) have transitional directions (Figure 4 and Table 1). Two R-polarity sites

(R3, R4) have an associated fission track age of ~1.1 Ma [*Booth et al.*, 2002]. An optically stimulated luminescence (OSL) date for sediments just east of site R4 indicate an age of ~250 ka [*Mahan et al.*, 2000]. OSL and thermal luminescence (TL) dates for sands and silts at Point Defiance (N11, N12, N19) and at the intersection of I-5 and Atlantic Street (N27, N28) indicate ages between 200 and 300 ka and of ~70 ka, respectively. OSL dates at Garfield Park in Tacoma (N17) and near Dash Point (N25) indicate ages >107 ka and ~180 ka, respectively [*Mahan et al.*, 2000].

[14] A 20-m-thick silt section near the eastern end of The Tacoma Narrows Bridge preserves part of a R-to-N transition. Similarly, at Wingehaven Park on Vashon Island, samples were collected above, below, and within a R-to-N polarity transition (Figure 5). Directions inferred as transitional were also found along the western shore of Tacoma Narrows (T13), along Puget Sound's eastern shore (T8, T11), and at the northern tip (T7) and along the western shore of Vashon Island (T2, T18; Figure 1).

[15] The site-mean statistics are often remarkably good for only three sample directions, although the overall dispersion of VGPs for both polarity groups ($S_{N + R} = 30°$) is significantly greater than a model value for the full range of secular variation at this latitude ($S_F = 17° ± 1°$ [*McFadden and McElhinny*, 1984]). Although the higher observed dispersion could have been caused by inaccuracies in the sediment recording process (e.g., bottom paleocurrents), differential vertical axis rotations, unrecognized or incorrect stratal tilts, unrecognized transitional directions, and/or unrecognized overprinting, the excess dispersion can also be attributed to higher within-site dispersion due to the low number of samples per site. The near-antipodal mean directions of the N- and R-polarity groups, however, indicate that PSV and other sources of error have been averaged out.

[16] Assuming that the silt deposits at sites with well-grouped sample directions ($\alpha_{95} < 15°$) reliably record PSV, the observed
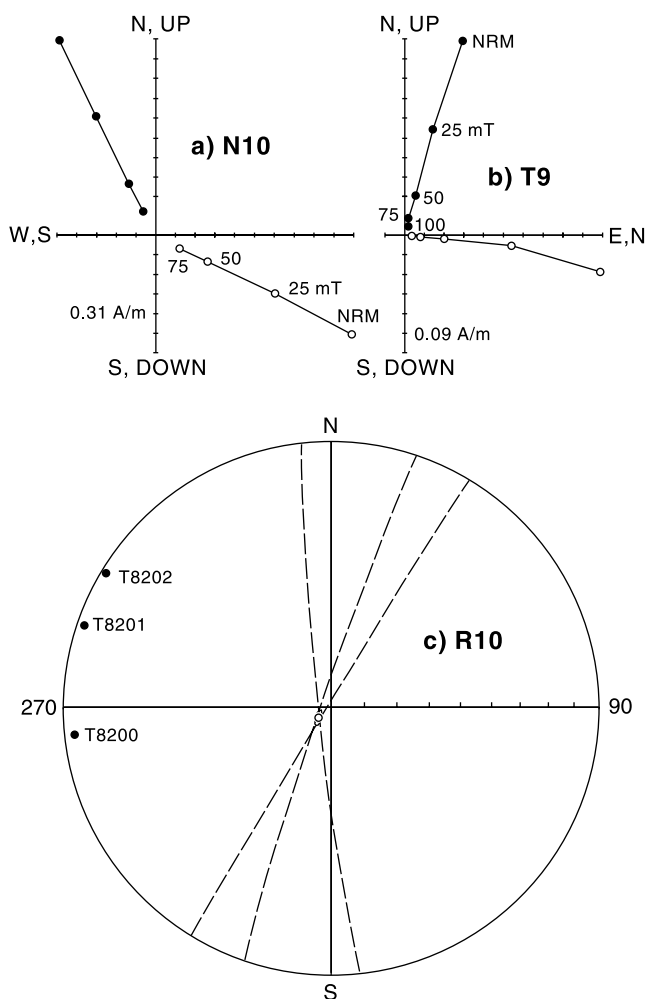
Figure 3. (a) Orthogonal projection of alternating field (AF) demagnetization vector endpoints for a sample from site N10 showing a univectorial normal-polarity remanent magnetization. (b) Vector plot of AF demagnetization data for a sample from site T9 showing a univectorial transitional-polarity magnetization. Solid symbols in both plots indicate projections onto the horizontal plane, and open symbols indicate projections onto the vertical plane. (c) Equal-area stereoplot showing intersecting remagnetization circles fitted to demagnetization data for samples from site R10. Dots indicate poles to the great circles projected from the lower hemisphere, and the open circle indicates the mean direction (reversed-polarity) for this site projected from the upper hemisphere. The intersection is tightly constrained, and the 95% confidence ellipse is correspondingly small.

paleomagnetic directions can be statistically compared with one another to estimate the relative likelihood of sites having similar directions due to coincidence or to significant agreement. *Bogue and Coe* [1981] initially developed a statistical method to correlate paleomagnetic directions from individual Columbia River basalt flows. Their method is based on the observation that the geomagnetic field direction at any given locality tends to be near the expected dipole field direction. Thus two similar but unusual directions away from the expected field direction are more likely acquired simultaneously than two similar directions near the expected direction. This technique is most accurate when applied over short periods of time relative to the frequency of PSV. In this

study, the period of time over which the sampled sediments were deposited is relatively long, so correlations indicated by the statistical comparison are less certain, and therefore only the strongest correlations are considered. In addition, the overall mean direction (Table 1) was substituted for the expected dipole field direction because the observed mean has a shallower inclination and a slightly more counterclockwise declination.

[17] In *Bogue and Coe*'s [1981] method, two hypotheses are tested. The "random" hypothesis (H_r) holds that similar paleomagnetic directions are random samplings of the geomagnetic field, and the "simultaneous" hypothesis (H_s) holds that the directions were acquired under the same geomagnetic field. The calculated probabilities (P) that similar paleomagnetic data (D) have arisen from either hypothesis ($P(D:H_r)$ or $P(D:H_S)$) are given in Table 2. $P(D:H_r)$ is calculated using a spherical distribution model based on *Fisher*'s [1953] probability function, and $P(D:H_S)$ is the significance level from *McFadden and Lowes*'s [1981] test of the null hypothesis stating that the two sample means are from populations having the same mean but different k (concentration) values. The ratios of $P(D:H_S)/P(D:H_r)$, also given in Table 2, indicate the relative likelihood of H_s versus H_r.

4. Discussion

[18] The fine-grained deposits of the Puget Lowland apparently record polarity and PSV of the geomagnetic field. As previously mentioned, however, a number of error sources might have affected the accuracy with which the fine-grained deposits recorded the ambient geomagnetic field. Paleocurrent alignment of magnetic grains is unlikely in lake bottom environments, and lake sediments have provided consistent and reproducible records of PSV in North America [*Lund*, 1996]. Vertical axis rotations are also unlikely in deposits this young, and although unrecognized stratal tilts could contribute to the error, they too would be relatively minor. The division between transitional directions and extreme PSV directions is arbitrary, and some of the highly dispersed N-polarity directions in Figure 4 might actually be transitional directions (see below). Unrecognized overprinted N-polarity directions are also unlikely because uniform unaltered sediments were sampled in which R-polarity and transitional directions were also found. Increased dispersion due to the low number of samples collected could not be avoided without greatly increasing the sampling time.

[19] The overall average inclinations for the fine-grained deposits (Table 1 and Figure 4) are also too shallow compared to the expected dipole field direction. The shallowing of inclinations is most likely due to compaction of the fine-grained lake sediments [*Anson and Kodama*, 1987], particularly in the older Quaternary deposits due to loading by ice sheets during the multiple Pleistocene glaciations. Because the degree of compaction is probably crudely similar at equivalent stratigraphic levels, comparisons of paleomagnetic directions to determine equivalent horizons are most likely valid.

[20] The transitional paleomagnetic directions for sites collected at Tacoma Narrows and at Wingehaven Park are plotted in Figure 5. Both of the stratigraphically lowest sites at Tacoma Narrows and Wingehaven Park have R polarity (R12, R18), and the highest site at Wingehaven Park has N polarity (N37). Intermediate directions at both localities are transitional, and clearly a R-to-N reversal is recorded in the fine-grained sediments. Directions at other sites with northerly declinations were considered transitional if their mean inclinations were <25°. The cut off value is arbitrary, however, and shallow-inclination N-polarity directions, such as those for sites N9, N15, and N27, might also be transitional directions.
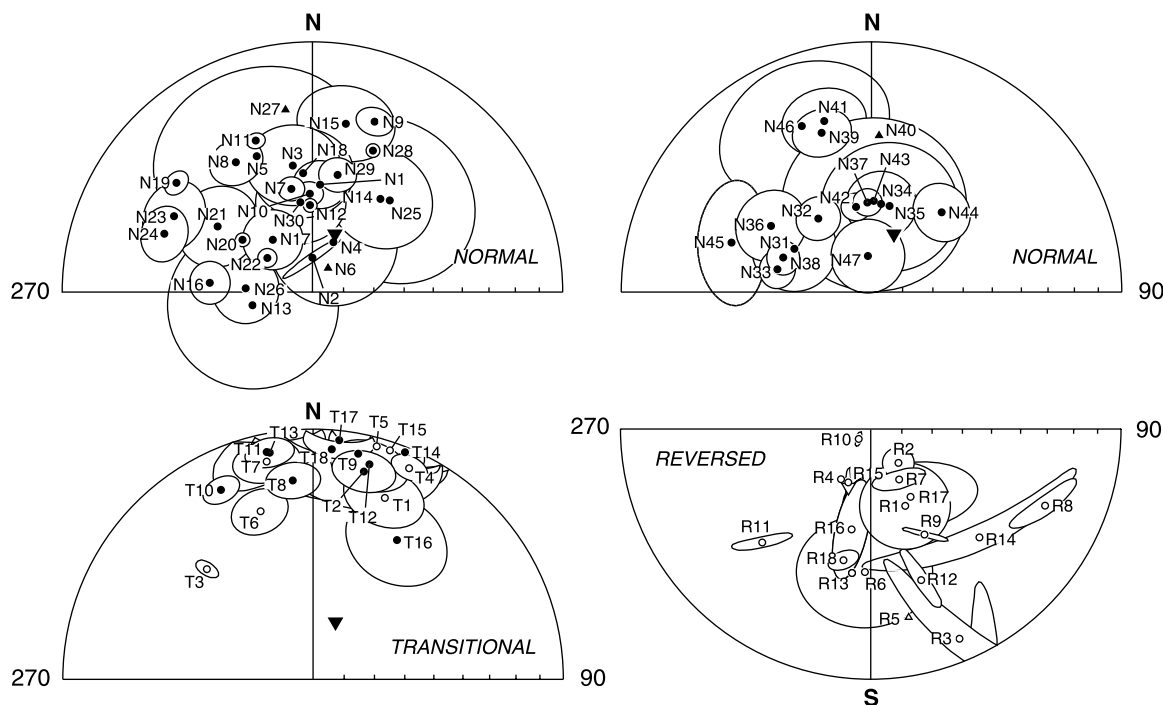
Figure 4. Equal-area stereoplots of normal-polarity, reversed-polarity, and transitional-polarity site-mean directions with their 95% confidence limits. Numbers are keyed to site data listed in Table 1. Solid circles are projected from the lower hemisphere, and open circles are projected from the upper hemisphere. Small triangles indicate site-mean directions with too few samples to calculate meaningful statistics (Table 1).

[21] Although the transitional directions could be associated with a number of subchrons within the Bruhnes polarity chron [*Champion et al.*, 1988], it is most likely related to the Bruhnes-Matuyama transition at ~780 ka. A fission track date on an interbedded tephra layer near site R4 indicates that Matuyama-aged sediments have been sampled there. A finite ^{14}C date of 44,880 ± 3050 ka near and stratigraphically above the eastern Tacoma Narrows locality [*Troost*, 1999] preclude these transitional directions from being related to the Laschamp event (~40 ka). Furthermore, the OSL and TL dates nearby and at Point Defiance (N11, N12, N19) between 200 and 300 ka indicate that the N-polarity sediments are below either the well-defined Jamaica (~180 ka) or Blake (~110 ka) events. Older subchrons have been proposed within the Bruhnes chron but are not as well established.

[22] Paleomagnetic correlations of the transitional directions also indicate that parts of the same geomagnetic reversal were sampled across the study area. The calculated probabilities and relative probabilities of the random (H_r) or simultaneous (H_s) hypotheses [*Bogue and Coe*, 1981] are given in Table 2. The first normal-polarity comparison in Table 2 is between site N1 (Figure 4) and nine other sites with similar directions. All of these directions are near the overall mean direction ($\delta < 20°$), and their relative probability values are correspondingly low (<40) and mixed between favoring H_r or H_s. In contrast, a correlation test between sites N9 and N15 indicates that H_s is more likely than H_r by a factor >9999, and so these two sites are probably within the same magnetostratigraphic horizon. Transitional directions at the east shore of Tacoma Narrows (T4, T5) are identical to those at Wingehaven Park (T14, T15), and that at Seahurst Park (T11) is widely correlated with directions at Redondo (T8), Peter Point on Vashon Island (T10), and on the west shore of Tacoma Narrows (T13). In addition, some of the northernmost N-polarity directions (N31, N33) are correlated with some of the southernmost sites (N16, N38).

[23] In Figure 6 the distribution of N-, transitional-, and R-polarity sites are shown superimposed on an aeromagnetic map of the central Puget Lowland [*Blakely et al.*, 1999]. Also shown are most of the calculated correlations between sites having relative probability factors for H_s of several thousand or more (Table 2). The aeromagnetic data show the local influence of human activity, such as The Tacoma Narrows Bridge (near T1 and N46) and at the Tacoma harbor docks (near R4). In addition, the pattern of N- and R-polarity sites near the southern end of Vashon Island appears to sharply define the southern limit of the Seattle uplift at its boundary with the adjacent Tacoma Basin (NW to SE line B). This boundary is also well defined by gravity and seismic tomography data [*Brocher et al.*, 2001].

[24] The pattern of paleomagnetic polarity (Figure 6) appears unrelated to the pattern of aeromagnetic anomalies, indicating that the anomalies are not due to differential uplift of strongly magnetized basement rocks such as the volcanic Crescent Formation. The polarity pattern is the result of the elevation of sites, past erosion, and tectonic movements. An estimate of the elevation of each site is given in Table 1 and clearly plays a role in polarity at the thick sections with transitional directions sampled at The Tacoma Narrows Bridge and Wingehaven Park. The N-polarity sites at Christiansen Road (N3–N6) on the western coast of Vashon Island, just across from R-polarity sites on beaches of the eastern Kitsap Peninsula (Figure 1), have much higher elevations (20–50 m). Moreover, N-polarity sites are always found above R-polarity sites, indicating that R-polarity subchrons within the Bruhnes chron have not been sampled.

[25] Deposition of fine-grained sediments over a surface with erosional relief might also account for the close proximity of N- and R-polarity sites, but it is difficult to evaluate because of limited exposures in the region. Tectonic uplift can cause the exposure of R-polarity sediments, and the majority of sites in
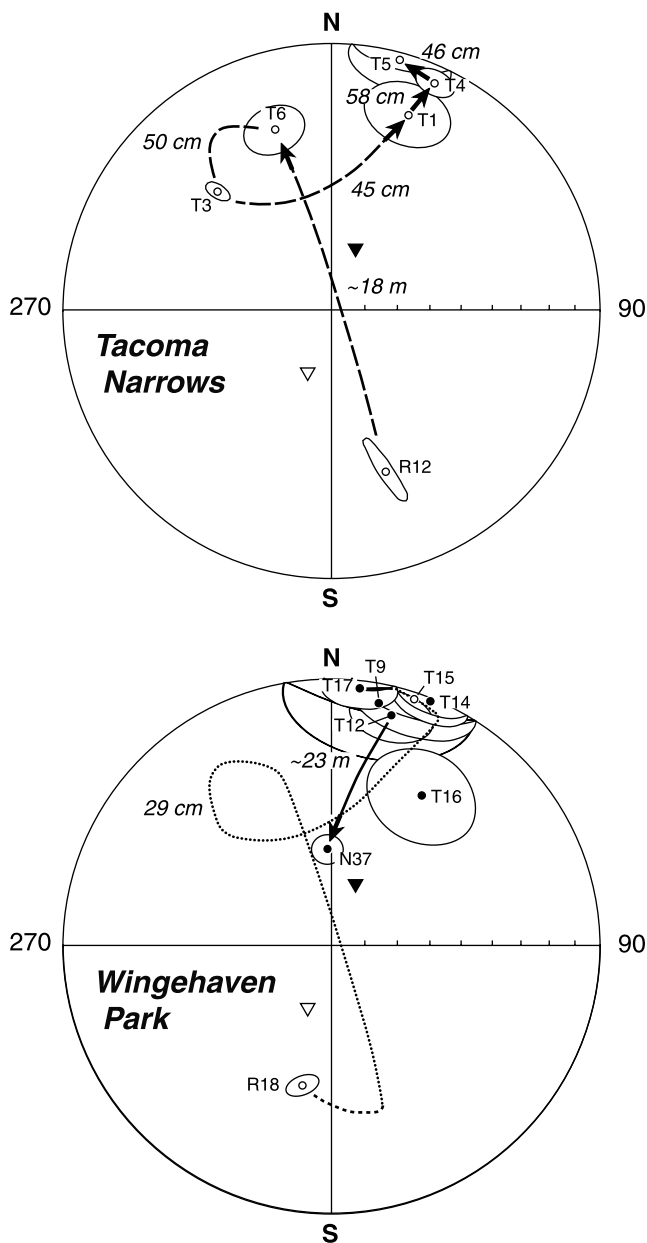
Figure 5. Equal-area stereoplot of site-mean directions for (a) a thick silt section just north of the eastern abutment of The Tacoma Narrows Bridge and (b) the section at Wingehaven Park (Figure 1). Sites R12 and R18 include the stratigraphically lowest samples at each site and have reversed-polarity mean directions. Site N37 is the stratigraphically highest site at Wingehaven Park and has a normal-polarity mean direction. Stratigraphic distances are indicated between sites as the paleomagnetic direction swings between reversed polarity and normal polarity; the path of the transition at Tacoma Narrows is shown by the dashed line. For comparison, that same path is superimposed on the Wingehaven Park data (dotted line), along with the apparent continuation of the transition to fully normal polarity (solid line). Inverted triangles indicate the normal and reversed directions of the present-day geomagnetic field in the central Puget Lowland.

such sediments over the Seattle uplift (Figure 6) indicate that uplift has continued since ~780 ka. The abrupt change in polarity across the southern boundary of the Seattle uplift might also indicate that the Tacoma fault intersects the land surface. In

addition, a dip-slip fault along the Tacoma Narrows is indicated by the down dropping of sites T13 and N46 on the west relative to sites R12, T1, and T3–T6 on the east.

[26] To determine the source of the aeromagnetic anomalies, gravity and magnetic profiles along line P to P′ (Figure 6) were fitted by a simple subsurface model shown in Figure 7. The fit of the gravity profile is constrained by SHIPS tomographic data indicating the depth to rocks having 4.5 km/s velocities [*Brocher et al.*, 2001], which is presumably the top of the Crescent Formation (Figure 7c). Not surprisingly, the fit to the gravity profile is excellent, but the concurrent fit to the magnetic profile (not shown), assuming a uniformly magnetized Crescent Formation, is poor. Slabs of reversely magnetized rock must be added to the model so that the calculated profile matches the observed magnetic profile (Figures 7a and 7c). Although the Crescent Formation is reversely magnetized at the surface in some places [*Beck and Engebretson*, 1982; *Globerman et al.*, 1982; *Wells and Coe*, 1985], locations of reversely magnetized rocks in Figure 7c are constrained only by the shape of the aeromagnetic data. In this model the Seattle fault is interpreted as a south dipping reverse fault and the southern margin of the Seattle uplift is interpreted as a south dipping ramp [*Pratt et al.*, 1997] (see Figure 7d). The reversely magnetized layers within the Crescent rocks also dip southward and might reflect stratigraphy within the formation.

5. Conclusions

[27] In this study paleomagnetic directions from fine-grained unaltered glacial and interglacial deposits have been used to define the area's magnetostratigraphy (Figures 1 and 6). Remarkably, the horizontal plane of sampled exposures (approximately sea level) intersects a R-to-N polarity transition that is most likely related to the Bruhnes-Matuyama geomagnetic reversal (Figure 5). Vertical adjustments on the order of ≤10 m could determine whether a sediment with N, R, or transitional directions was sampled. The transitional horizon is at least 2 m thick and serves well as a stratigraphic marker horizon within the previously undated sediments between the Salmon Springs and Double Bluff glacial deposits (Figure 2).

[28] Seismic reflection data analyzed by *Pratt et al.* [1997] image subsurface structure to depths of several km, whereas seismic tomography [*Brocher et al.*, 2001] does so to depths of 25–30 km. In Figure 8, cross sections of the Puget Lowland are shown depicting the thin- and thick-skinned structural models for the region based on the reflection and tomographic techniques, respectively. Overall, the paleomagnetic data conform to the Seattle uplift: R-polarity sites are mostly found above this structural feature (Figure 7). The sharp boundary between the N- and R-polarity data along the Seattle uplift's southern edge (line B, Figure 6) is consistent with a fault structure (Tacoma fault?) that apparently reaches the surface. The paleomagnetic correlation of transitional and N-polarity sites in the southern part of the study area with sites in the northern part, however, implies less deformation of the Pleistocene sediments than of the underlying Tertiary deposits.

[29] Regional deformation of the Puget Lowland is a result of the ongoing convergence of the Juan de Fuca and North American plates expressed through both faulting and folding. Active faults in the Puget Lowland have been inferred to offset Quaternary deposits, and although only the Seattle fault has had a clear history of late Holocene surface rupture [*Nelson et al.*, 1999], future major earthquakes are certain to occur within the region. The location and nature of active faults, as well as the overall structure beneath the Puget Lowland, are at present still open questions, and more work is needed to decipher the region's complex structural setting and paleoseismicity.

Table 2. Site-Mean Correlations Based on the Statistical Method of *Bogue and Coe* [1981][a]

Site	k	δ	α	$P(D{:}H_r)$	$P(D{:}H_s)$	Relative Probability	
			Normal Polarity				
N1[b]	224	11.3					
N3	76	11.0	11.0	0.4005	0.1015	H_r,	4
N7	902	3.1	8.9	0.2058	0.0214	H_r,	10
N10	752	7.5	4.5	0.0202	0.2647	H_s,	13
N12	2782	8.7	7.6	0.1196	0.0320	H_r,	4
N29	427	18.0	6.8	0.0811	0.1003	H_s,	1
N30	76	5.3	8.2	0.1557	0.2349	H_s,	2
N34	120	11.5	6.7	0.0770	0.2585	H_s,	3
N37	724	7.7	7.1	0.0943	0.0648	H_r,	1
N42	681	5.1	10.6	0.3594	0.0098	H_r,	37
N8[b]	233	20.0					
N11	1897	21.3	8.5	0.0007	0.0181	H_s,	26
N39	208	23.5	11.5	0.0086	0.0208	H_s,	2
N41	100	27.5	15.2	0.0830	0.0157	H_r,	5
N9[b]	559	38.3					
N15	78	31.6	8.3	<0.0001	0.1799	H_s,	>9999
N17[b]	161	14.9					
N22	1606	20.9	6.1	0.0145	0.1484	H_s,	10
N32	306	10.7	8.5	0.0528	0.0819	H_s,	2
N21[b]	88	22.9					
N20	2931	19.3	9.5	0.0084	0.0827	H_s,	10
N36	111	24.6	12.0	0.0249	0.8461	H_s,	34
N23[b]	128	36.0					
N19	1061	35.7	10.2	<0.0001	0.0333	H_s,	>3330
N24	220	40.0	5.9	<0.0001	0.3348	H_s,	>9999
N45	33	37.7	8.5	<0.0001	0.4662	H_s,	>9999
N33[b]	404	30.7					
N16	336	35.7	5.0	<0.0001	0.1895	H_s,	>9999
N31	80	23.0	7.7	<0.0001	0.2281	H_s,	>9999
N38	512	27.2	3.6	<0.0001	0.3886	H_s,	>9999
			Transitional Polarity				
T2[b]	213	47.6					
T12	144	51.0	3.4	<0.0001	0.6446	H_s,	>9999
T5[b]	112	664					
T4	647	72.9	9.7	<0.0001	0.0613	H_s,	>6130
T14	195	63.2	9.1	<0.0001	0.1299	H_s,	>9999
T15	73	67.0	3.4	<0.0001	0.8041	H_s,	>9999
T6[b]	228	87.1					
T7	212	69.0	18.9	<0.0001	0.0012	H_s,	>120
T11[b]	42	48.7					
T8	284	36.6	14.0	<0.0001	0.0938	H_s,	>9380
T10	590	40.2	16.4	<0.0001	0.0445	H_s,	>4450
T13	383	49.2	0.7	<0.0001	0.9916	H_s,	>9999
			Reversed Polarity				
R1[b]	27	6.9					
R9	6140	8.9	11.6	0.3665	0.0984	H_r,	4
R17	28	8.8	2.2	0.0162	0.9626	H_s,	59
R2[b]	226	21.0					
R7	419	15.1	5.9	<0.0001	0.0850	H_s,	>8500
R4[b]	14719	23.7					
R15	6476	21.6	2.3	<0.0001	0.0068	H_s,	>680
R13	27220	21.1					
R16	140	14.2	14.0	0.0060	0.0004	H_r,	17
R18	514	20.8	6.4	0.0309	0.0024	H_r,	13

[a] Site, number keyed to sequence in Table 1; k is the concentration parameter [*Fisher*, 1953], for those means with Bingham statistics the large of the two Bingham concentration parameter is used; δ is the angular distance between the site-mean and the observed N + R means (*I/D*: 57°/343° and −57°/163°); α is the angular distance between the two paleomagnetic directions; $P(D{:}H_r)$ and $P(D{:}H_s)$ are the probabilities of similar paleomagnetic directions (*D*) assuming the random and simultaneous hypotheses (H_r and H_s), respectively. Relative probability indicates which hypothesis is favored and the factor of its likelihood. Modified from the method of *Bogue and Coe* [1981] (see text).
[b] Site-mean direction to which other directions are compared.
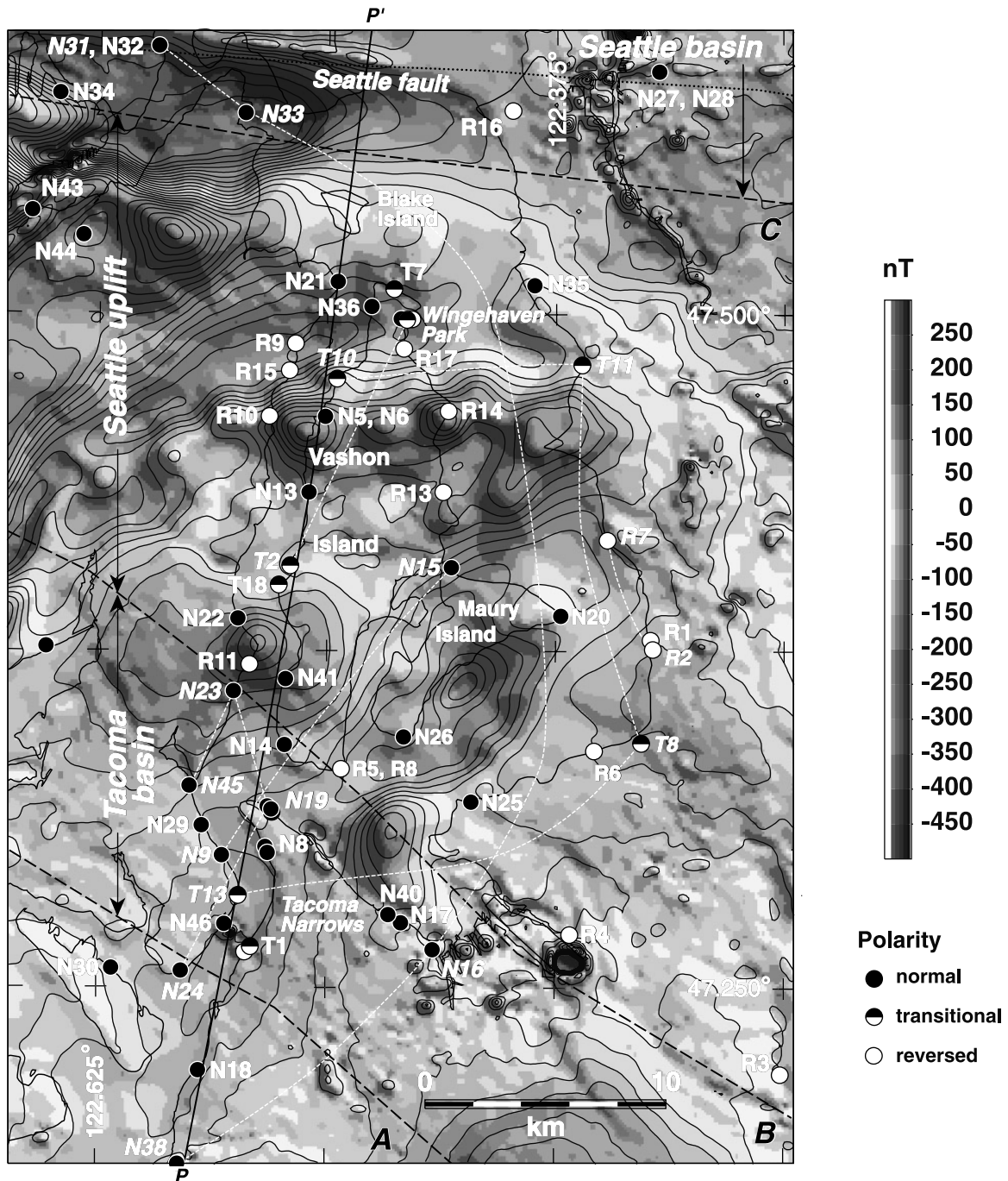
Figure 6. Map of the central Puget Lowland showing sampling sites and magnetic polarities (as in Figure 1) superimposed on an aeromagnetic map for the region [*Blakely et al.*, 1999]. Bold dashed lines (B and C) indicate the margins of the Seattle uplift and the limit (A) of the southward dipping ramp at the southern edge of the uplift [after *Pratt et al.*, 1997]. The dotted line north of the Seattle uplift marks the trace of the Seattle fault. Fine dashed lines connect sites that have been statistically correlated based on their atypical, but similar, paleomagnetic directions (Table 2). See color version of this figure at back of this issue.
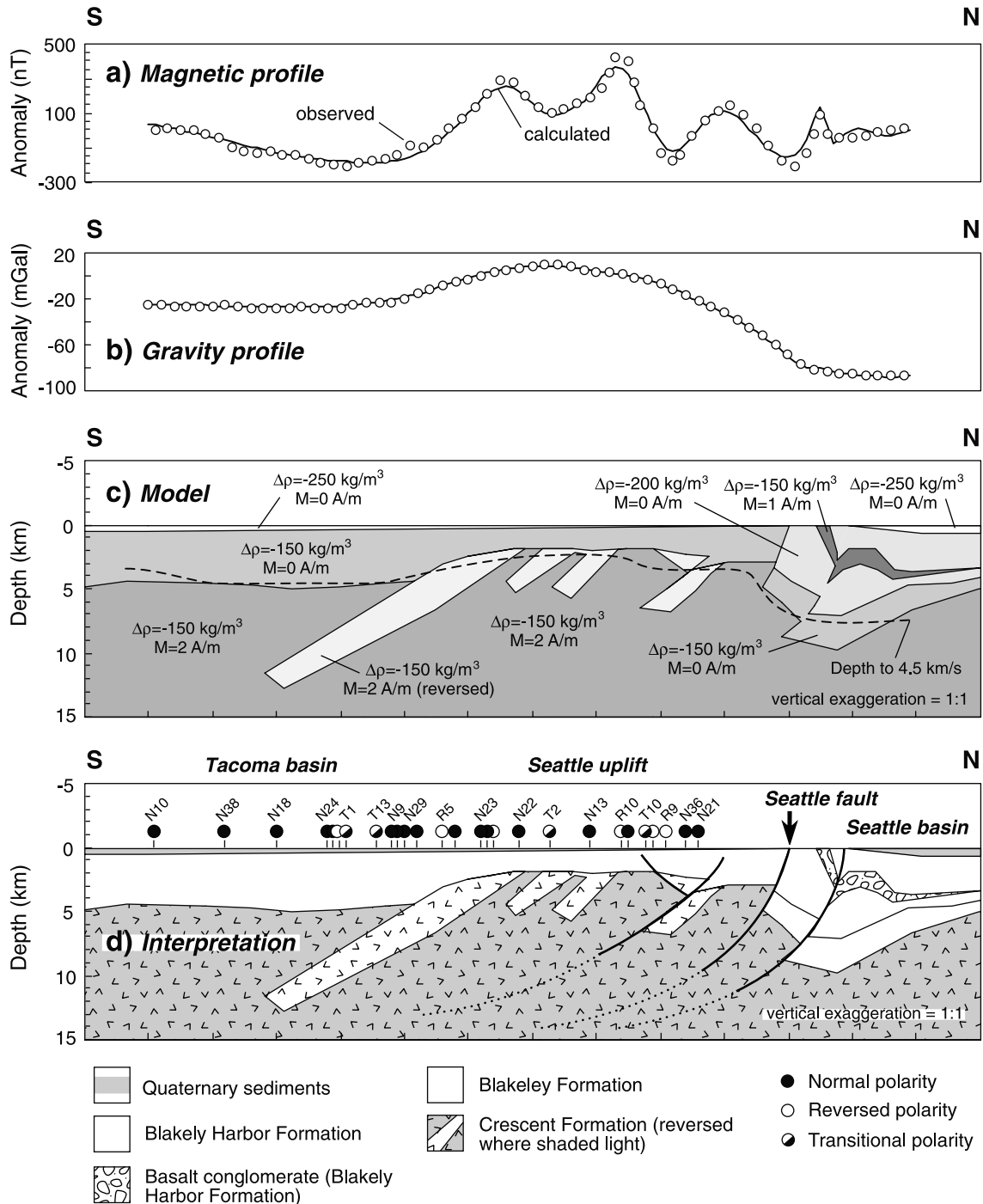
Figure 7. North to south (a) magnetic [*Blakely et al.*, 1999] and (b) gravity [*Brocher et al.*, 2001] profiles (line P-P′ in Figure 6) across the south central Puget Lowland. (c) A model in which seismic tomography data (depth to 4.5 km/s velocity rocks) are used to constrain the gravity fit and reversed-polarity slabs of Crescent Formation are used to fit the magnetic profile. (d) Interpretation of the model with the Seattle fault as a south dipping reverse fault and the southern margin of the Seattle uplift as possibly a south dipping ramp. Thickness of the thin layer of Quaternary sediments in Figures 7c and 7d is based on data from *Jones* [1996].
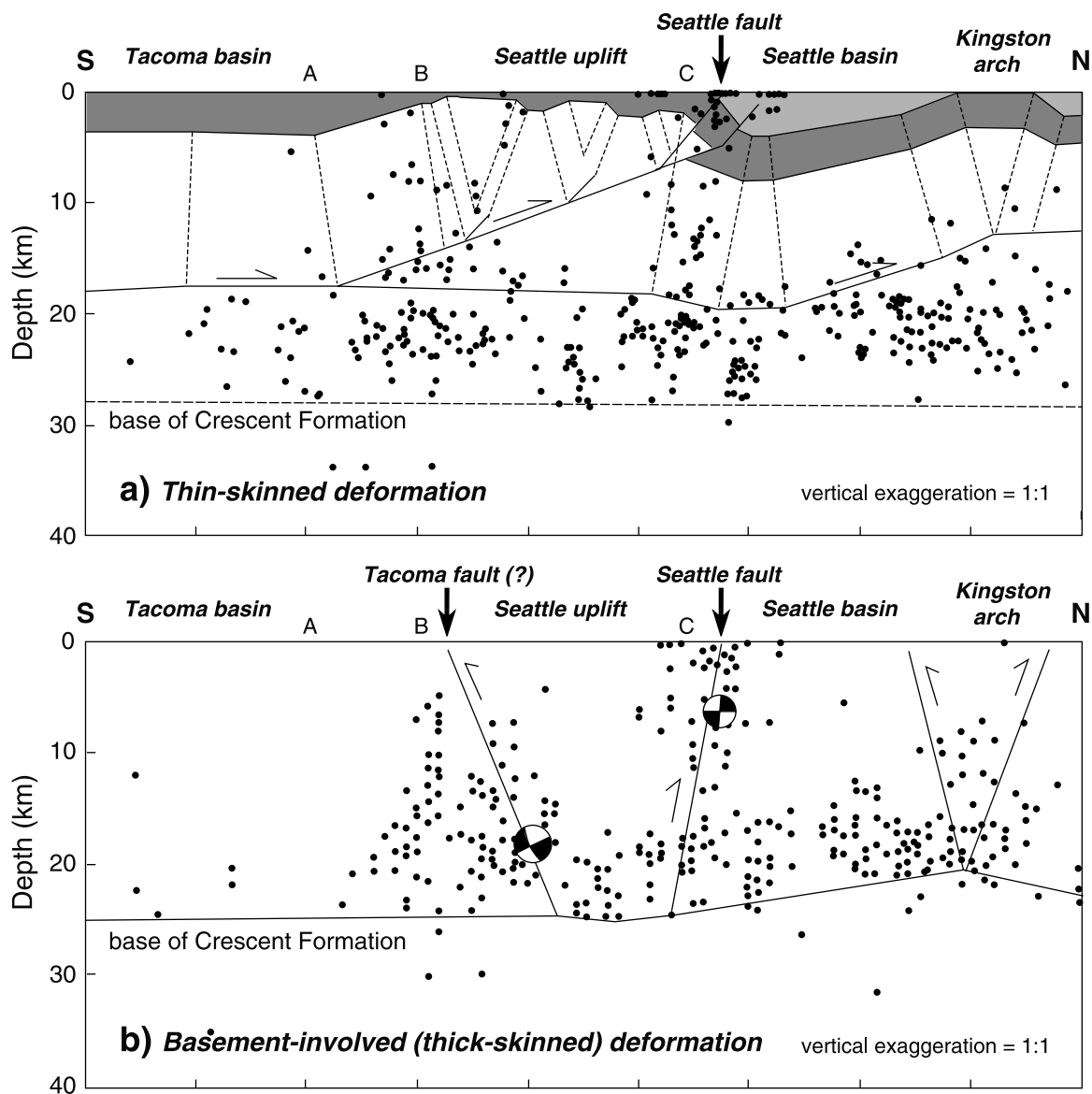
Figure 8. North-to-south cross sections beneath the central Puget Lowland based on (a) seismic reflection profiles analyzed by *Pratt et al.* [1997] and (b) the three-dimensional seismic velocity model of *Brocher et al.* [2001]. Dots indicate hypocenters of local earthquakes projected E-W onto the cross sections. In Figure 8a a thin-skinned model is shown in which the Seattle fault is a thrust fault that shallows with depth and merges with a midcrustal decollement. Light shaded areas indicate Miocene and younger deposits, and darker shaded areas indicate Eocene and Oligocene deposits [after *Pratt et al.*, 1997]. In Figure 8b a thick-skinned deformational model is shown in which the steeply dipping Seattle and Tacoma faults bound the Seattle uplift to the north and south, respectively. The steeply dipping faults connect at high angles with a lower crustal decollement at the base of the Crescent Formation. Focal mechanisms for the 1995 $M = 5$ Point Robinson and the 1997 $M = 5$ Bremerton earthquakes are also shown and are interpreted as having occurred on the Tacoma and Seattle faults, respectively [after *Brocher et al.*, 2001].
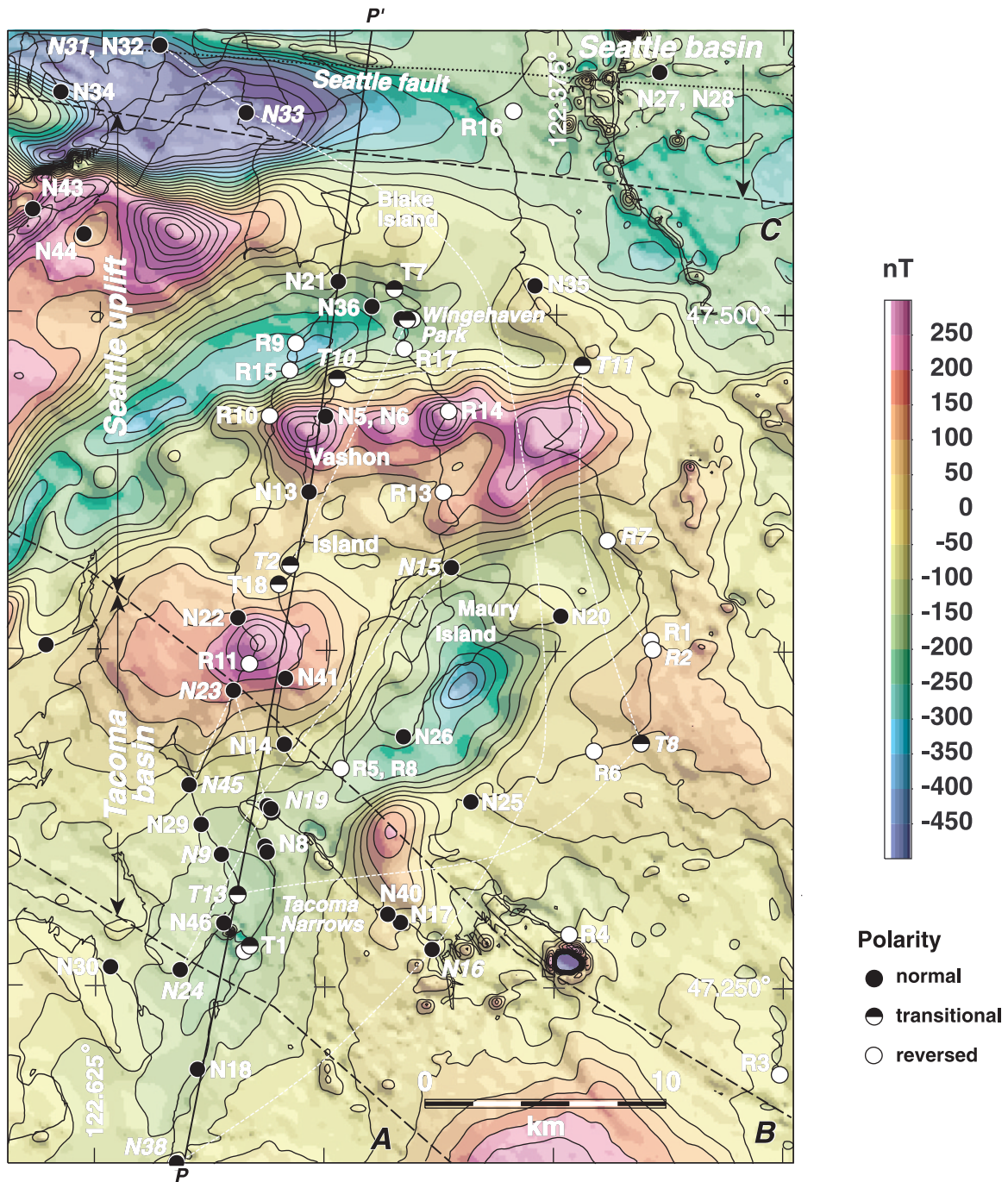
References

Anson, G. L., and K. P. Kodama, Compaction-induced inclination shallowing of the post-depositional remanent magnetization in a synthetic sediment, *Geophys. J. R. Astron. Soc.*, *88*, 673–692, 1987.

Atwater, B. F., and E. Hemphill-Haley, Recurrence intervals for great earthquakes of the past 3,500 years at northeastern Willapa Bay, Washington, *U.S. Geol. Surv. Prof. Pap.*, *1576*, 108 pp., 1997.

Beck, M. E., Jr., and D. C. Engebretson, Paleomagnetism of small basalt exposures in the west Puget Sound area, Washington, and speculations on the accretionary origin of the Olympic Mountains, *J. Geophys. Res.*, *87*, 3755–3760, 1982.

Blakely, R. J., R. E. Wells, and C. S. Weaver, Puget Sound aeromagnetic maps and data, *U.S. Geol. Surv. Open File Rep.*, *99-514*, 1999. (Available at http://geopubs.wr.usgs.gov/open-file/of 99-514)

Blunt, D. J., D. J. Easterbrook, and N. W. Rutter, Chronology of Pleistocene sediments in the Puget Lowland, Washington, *Bull. Wash. Div. Geol. Earth Resour.*, *77*, 321–353, 1987.

Bogue, S. W., and R. S. Coe, Paleomagnetic correlation of Columbia River Basalt flows using secular variation, *J. Geophys. Res.*, *86*, 11,883–11,897, 1981.

Booth, D. B., Timing and processes of deglaciation along the southern margin of the Cordilleran Ice Sheet, in *The Geology of North America*, vol. K-3, *North America and Adjacent Oceans During the Last Deglaciation*, edited by W. F. Riddiman and H. E. Wright Jr., pp. 71–90, Geol. Soc. of Am., Boulder, Colo., 1987.

Booth, D. B., H. H. Waldron, and K. G. Troost, Geologic map of the Poverty Bay 7.5-minute quadrangle, *U.S. Geol. Surv. Open File Rep*, in press, 2002.

Brocher, T. M., T. Parsons, R. E. Blakely, N. I. Christensen, M. A. Fisher, and R. E. Wells, Upper crustal structure in Puget Lowland, Washington: Results from the 1998 seismic hazards investigation in Puget Sound, *J. Geophys. Res.*, *106*, 13,541–13,564, 2001.

Bucknam, R. C., E. Hemphill-Haley, and E. B. Leopold, Abrupt uplift within the past 1700 years at southern Puget Sound, Washington, *Science*, *258*, 1611–1614, 1992.

Champion, D. E., M. A. Lanphere, and M. A. Kuntz, Evidence for a new geomagnetic reversal from lava flows in Idaho: Discussion of short polarity reversals in the Bruhnes and late Matuyama polarity chrons, *J. Geophys. Res.*, *93*, 11,667–11,680, 1988.

Crandell, D. R., D. R. Mullineaux, and H. H. Waldron, Pleistocene sequence in the southeastern part of the Puget Sound lowland, Washington, *Am. J. Sci.*, *256*, 384–397, 1958.

Easterbrook, D. J., Chronology of pre-Late Wisconsin Pleistocene sediments in the Puget Lowland, Washington, *Bull. Wash. Div. Geol. And Earth Res.*, *80*, 191–206, 1994.

Easterbrook, D. J., D. R. Crandell, and E. B. Leopold, Pre-Olympia Pleistocene stratigraphy and chronology in the central Puget Lowland, Washington, *Geol. Soc. Am. Bull.*, *78*, 13–20, 1967.

Easterbrook, D. J., J. L. Roland, R. J. Carson, and N. D. Naeser, Application of paleomagnetism, fission-track dating, and tephra correlation to Lower Pleistocene sediments in the Puget Lowland, Washington, in *Dating Quaternary Sediments*, edited by D. J. Easterbrook, *Spec. Pap. Geol. Soc. Am.*, *227*, 139–165, 1988.

Fisher, R. A., Dispersion on a sphere, *Proc. R. Soc. London, Ser. A*, *217*, 295–305, 1953.

Globerman, B. R., M. E. Beck Jr., and R. A. Duncan, Paleomagnetism and tectonic significance of Eocene basalts from the Black Hills, Washington Coast Range, *Geol. Soc. Am. Bull.*, *93*, 1151–1159, 1982.

Johnson, S. Y., C. J. Potter, and J. M. Armentrout, Origin and evolution of the Seattle basin and Seattle fault, *Geology*, *22*, 71–74, 1994.

Johnson, S. Y., C. J. Potter, J. M. Armentrout, J. J. Miller, C. Finn, and C. S. Weaver, The southern Whidbey Island fault, an active structure in the Puget Lowland, Washington, *Geol. Soc. Am. Bull.*, *108*, 334–354, 1996.

Johnson, S. Y., S. V. Dadisman, J. R. Childs, and W. D. Stanley, Active tectonics of the Seattle fault and central Puget Sound, Washington—Implications for earthquake hazards, *Geol. Soc. Am. Bull.*, *111*, 1042–1053, 1999.

Jones, M. A., Thickness of unconsolidated deposits in the Puget Sound Lowland, Washington and British Columbia, *U.S. Geol. Surv. Water Res. Invest. Rep.*, *94–4133*, 1996.

Kirschvink, J. L., The least-squares line and plane and analysis of palaeomagnetic data, *Geophys. J. R. Astron. Soc.*, *62*, 699–718, 1980.

Ludwin, R. S., C. S. Weaver, and R. S. Crosson, Seismicity of Washington and Oregon, in *The Geology of North America*, vol. 1, *Neotectonics of North America*, edited by D. B. Slemmons et al., pp. 77–98, Geol. Soc. of Am., Boulder, Colo., 1991.

Lund, S. P., A comparison of Holocene paleomagnetic secular variation records from North America, *J. Geophys. Res.*, *101*, 8007–8024, 1996.

Mahan, S. A., D. B. Booth, and K. G. Troost, Luminescence dating of glacially derived sediments: A case study for the Seattle Mapping Project (abstract), *Geol. Soc. Am. Abstr. Programs*, *32*, A–27, 2000.

McFadden, P. L., and F. J. Lowes, The discrimination of mean directions drawn from Fisher distributions, *Geophys. J. R. Astron. Soc.*, *67*, 19–33, 1981.

McFadden, P. L., and M. W. McElhinny, A physical model for palaeosecular variation, *Geophys. J. R. Astron. Soc.*, *78*, 809–830, 1984.

Nelson, A. R., S. K. Pezzopane, R. C. Bucknam, R. D. Koehler, C. F. Narwold, H. M. Kelsey, W. T. Laprade, R. E. Wells, and S. Y. Johnson, Holocene surface faulting in the Seattle fault zone, Bainbridge Island, Washington (abstract), *Seismol. Res. Lett.*, *70*, 223, 1999.

Onstott, T. C., Application of the Bingham distribution function in paleomagnetic studies, *J. Geophys. Res.*, *85*, 1500–1510, 1980.

Pratt, T. L., S. Johnson, C. Potter, W. Stepenson, and C. Finn, Seismic reflection images beneath Puget Sound, western Washington State: The Puget Lowland thrust sheet hypothesis, *J. Geophys. Res.*, *102*, 27,469–27,489, 1997.

Richmond, G. M., and D. S. Fullerton, Introduction to Quaternary glaciations of the United States of America, *Quat. Sci. Rev.*, *5*, 3–10, 1986.

Rogers, A. M., T. J. Walsh, W. J. Kockelman, and G. R. Priest, Earthquake hazards in the Pacific Northwest—An overview, in *Assessing Earthquake Hazards and Reducing Risk in the Pacific Northwest*, edited by A. M. Rogers et al., *U.S. Geol. Surv. Prof. Pap.*, *1560*, 1–54, 1996.

Smith, J. G., Geologic map of upper Eocene to Holocene volcanic and related rocks in the Cascade Range, Washington, *U.S. Geol. Surv. Misc. Invest.Map I-2005*, scale 1:500,000, 1993.

Troost, K. G., The Olympia nonglacial interval in the South-central Puget Lowland, M.S. thesis, 123 pp., Univ. of Wash., Seattle, 1999.

Troost, K. G., and D. B. Booth, The Seattle geologic mapping project (abstract), *Geol. Soc. Am., Abstr. Programs*, *31*, A-79, 1999.

Wells, R. E., and R. S. Coe, Paleomagnetism and geology of Eocene volcanic rocks of southwest Washington: Implications for mechanisms of tectonic rotation, *J. Geophys. Res.*, *90*, 1925–1947, 1985.

Wells, R. E., and C. S. Weaver, Block deformation in Puget Lowland, in *Proceedings of the National Earthquake Prediction Evaluation Council*, edited by V. E. Frizzel, *U.S. Geol. Surv. Open File Rep.*, *93–333*, 14–16, 1993.

Wells, R. E., C. S. Weaver, and R. J. Blakely, Fore arc migration in Cascadia and its neotectonic significance, *Geology*, *26*, 759–762, 1998.

R. J. Blakely, U.S. Geological Survey, 345 Middlefield Road, Mail Stop 989, Menlo Park, CA 94025, USA. (blakely@usgs.gov)

D. B. Booth, Department of Earth and Space Sciences, University of Washington, Box 352700, Seattle, WA 98195, USA. (dbooth@u.washington.edu)

J. T. Hagstrum, U.S. Geological Survey, 345 Middlefield Road, Mail Stop 937, Menlo Park, CA 94025, USA. (jhag@usgs.gov)

K. G. Troost, Department of Geological Sciences, University of Washington, Box 351310, Seattle, WA 98195, USA. (ktroost@u.washington.edu)

Figure 6. Map of the central Puget Lowland showing sampling sites and magnetic polarities (as in Figure 1) superimposed on an aeromagnetic map for the region [*Blakely et al.*, 1999]. Bold dashed lines (B and C) indicate the margins of the Seattle uplift and the limit (A) of the southward dipping ramp at the southern edge of the uplift [after *Pratt et al.*, 1997]. The dotted line north of the Seattle uplift marks the trace of the Seattle fault. Fine dashed lines connect sites that have been statistically correlated based on their atypical, but similar, paleomagnetic directions (Table 2).